Organic Electronics 39 (2016) 59–63

Contents lists available at ScienceDirect

Organic Electronics

journal homepage: www.elsevier.com/locate/orgel

Letter

Integrating nanostructured electrodes in organic photovoltaic devices for enhancing near-infrared photoresponse

Alexandre M. Nardes [a], Sungmo Ahn [b], Devin Rourke [b], Chenchen Mao [b], Jao van de Lagemaat [a], Andrew J. Ferguson [a, *], Wounjhang Park [b, c], Nikos Kopidakis [a, d, **]

[a] National Renewable Energy Laboratory, 15013 Denver West Parkway, Golden, CO 80401, USA
[b] Department of Electrical, Computer, and Energy Engineering, University of Colorado, Boulder, CO 80309-0425, USA
[c] Materials Science and Engineering Program, University of Colorado, Boulder, CO 80303, USA
[d] Department of Engineering, Macquarie University, NSW, 2109, Australia

ARTICLE INFO

Article history:
Received 1 April 2016
Received in revised form
2 August 2016
Accepted 10 September 2016

Keywords:
Organic photovoltaics
Photonic electrodes
Nanostructured electrodes
Plasmons
Surface plasmon polaritons

ABSTRACT

We introduce a simple methodology to integrate prefabricated nanostructured-electrodes in solution-processed organic photovoltaic (OPV) devices. The tailored "photonic electrode" nanostructure is used for light management in the device and for hole collection. This approach opens up new possibilities for designing photonically active structures that can enhance the absorption of sub-bandgap photons in the active layer. We discuss the design, fabrication and characterization of photonic electrodes, and the methodology for integrating them to OPV devices using a simple lamination technique. We demonstrate theoretically and experimentally that OPV devices using photonic electrodes show a factor of ca. 5 enhancement in external quantum efficiency (EQE) in the near infrared region. We use simulations to trace this observed efficiency enhancement to surface plasmon polariton modes in the nanostructure.

1. Introduction

The development of low bandgap, light-harvesting copolymers has enabled single-junction OPV devices to surpass the 10% power conversion efficiency (PCE) mark [1,2]. Further enhancements of OPV performance are likely to require the design and optimization of device architectures, including the use of multiple junctions [2] and photonic/plasmonic elements [3–5]. The latter opens up the possibility to broaden the spectral response of single-junction OPV due to enhanced light harvesting by weak, sub-bandgap absorptions due to, for instance, charge-transfer (CT) states [6–11]. Sensitive EQE measurements, coupled with the measured optical properties of the device stack, suggest that the *internal* quantum efficiency (IQE) for many OPV active layers remains high (and constant) even at photon energies much smaller than the optical bandgap of the active materials [11]. The observation of efficient carrier generation from CT states has been suggested as a paradigm-shifting route to a new efficiency regime for OPV [12].

Efforts to exploit photonic/plasmonic elements in OPV devices have included a number of different strategies [3–5]. These include incorporation of metallic nanoparticles into the device architecture or sandwiching the active layer and carrier transport layers in a metallic nanocavity [13,14], which enhance the optical and photovoltaic properties as a result of strong near-field coupling to a localized surface plasmon resonance (LSPR) and/light scattering effects. More recently, research has focused on the use of patterned metal electrodes, which provide a greater degree of control/flexibility and can be designed to couple incident solar radiation into surface plasmon polariton (SPP) modes or waveguide modes that propagate laterally through the active layer [3–5]. There have been several pioneering theoretical [15,16] and experimental [17–22] studies of the incorporation of random and periodic patterned metal electrodes into OPV devices, several of which aim to extend the spectral response of the active layer further into the near-infrared (NIR) [18–22]. Early, pioneering efforts to include such structures demonstrated the viability of such a strategy, but the sub-bandgap EQE enhancement was limited either by use of a non-optimal grating period that resulted in excitation of higher SPP

* Corresponding author.
** Corresponding author. Department of Engineering, Macquarie University, NSW, 2109, Australia.
E-mail addresses: andrew.ferguson@nrel.gov (A.J. Ferguson), nikos.kopidakis@mq.edu.au (N. Kopidakis).

http://dx.doi.org/10.1016/j.orgel.2016.09.011
1566-1199/

modes [18,20] or the reduced transparency of the nanostructured electrode [19,22].

We have previously shown by a combined optical and electrical simulation of the device performance that NIR photocurrent enhancement can be achieved by using a metal nanograting as the back electrode [16]. Our simulations showed that excitation of SPPs in the grating enhances the optical field in the active layer and that the grating can be designed so that the enhancement occurs in the near-infrared where the normal absorption in the active layer is low [16]. Here we experimentally realize this device and demonstrate that enhancement of the EQE is indeed observed in the spectral region predicted by the simulation. This confirms the power of simulation to design gratings that target optical field enhancement in a specific wavelength range of interest that can be focused in the active layer. We present a methodology for fabricating gratings by laser interference lithography (LIL) and a simple lamination technique for integrating them as back electrodes in an OPV device [23,24]. We demonstrate reasonable sub-bandgap EQE enhancement factors (>2 even for non-optimal incident light polarization) using the prototypical P3HT:PCBM active layer. However, the overall device performance is limited by the need to include an adhesive layer to bond the pre-fabricated grating electrode to the active layer. With that said, we anticipate that this current limitation could be circumvented by the use of a more appropriate adhesive layer, and that the strategy demonstrated here could be universally applied to any OPV active layer.

2. Experimental

The nanostructured-Ag electrodes were fabricated by the LIL technique, which is cost-effective and also scalable to larger volume production [25,26]. First, a 200 nm thick Ag layer was thermally evaporated onto a 125 μm thick polyethylene terephthalate (PET) flexible substrate. A thin photoresist layer was spin coated on top of the Ag film, and exposed under the sinusoidal laser interference pattern formed uniformly over large area by a custom-built Lloyd's interferometer. We used a 325 nm He-Cd laser as a light source with sufficient coherence length. Precise control of the baking, exposure, and development conditions made it possible to obtain one-dimensional grating patterns with slight undercut in the resist layer. A 20 nm thick Ag layer was evaporated on top of the developed photoresist pattern, which, after an acetone lift-off step, resulted in highly uniform one-dimensional Ag gratings over an area of ~1 cm^2.

Inverted OPV devices, without a top electrode, had the structure glass/ITO/ZnO/P3HT:PCBM and were fabricated as reported previously [23]. A glass slide with patterned ITO was sonicated in acetone and isopropyl alcohol, and subsequently treated with an oxygen plasma for 5 min. Zinc oxide (ZnO) is deposited by spin coating a diethylzinc solution mixed with tetrahydrofuran, followed by thermal conversion at 120 °C in air. The Glass/ITO/ZnO substrates are transferred to a N_2-filled glove box for the active layer deposition. The active layer was ~250 nm thick and was spin coated from a 1:1 wt ratio solution of P3HT:PCBM dissolved in dichlorobenzene.

To complete the device, an adhesive layer is required on the nanostructured-Ag/PET substrates [23]. For this we used a P3HT solution in dichlorobenzene with 10% by weight d-sorbitol, spin coated on the nanostructured-Ag surface. The two parts of the device are then brought together and placed in a hydraulic hot press for lamination in air, to complete the device stack: Glass/ITO/ZnO/P3HT:PCBM//P3HT:sorbitol/Ag/PET, where "//" denotes the laminated interface. Both the top and bottom plates of the press are preheated to 130 °C. The sample is kept on the bottom plate for 10 min and then pressed with 1.9 MPa for an additional 10 min. Control devices were fabricated at the same time with the same procedure using flat-Ag electrodes.

The EQE of the devices was measured under short circuit conditions with a Newport Oriel IQE200 system, using lock-in detection.

3. Results and discussion

3.1. Nanostructured electrode design and fabrication

Enhanced NIR photoresponse in OPV devices based on the P3HT:PCBM active layer has been previously demonstrated using quasi-random [19] and periodic [18,21] patterned metal electrodes. In the former case, the overall performance of the device at wavelengths above the optical bandgap is limited by the transmittance of the partially transparent gold layer, whereas the latter employ periodic gratings formed by direct nanoimprint lithography of the active layer, but result in EQE enhancement factors less than 2.5.

Similar to previous work [21], we chose to design a simple, and thus easy to fabricate, nanostructure comprising a periodic surface grating where the SPP mode is positioned in the NIR spectral region. We use the finite element method (FEM) in the commercial package COMSOL Multiphysics to simulate the optical field distribution in the whole device stack. The simulation takes as inputs the *n* & *k* spectra of each layer and the solar spectrum, and numerically solves Maxwell's equations for the steady-state electric field profile within the active layer [16]. The thickness of each of the flat layers on the device stack (ITO, ZnO and active layer) is fixed to the experimental values and the parameters that are allowed to vary to tune the position of the SPP resonance are the depth (height), duty ratio, and period of the grating (the linewidth of the grating feature is determined by the product of the duty ratio and grating period). Periodic boundary conditions are imposed (along the x-direction in Fig. 1) in such a way that the two-dimensional simulation cell has width equal to the nanostructured grating periodicity.

Fig. 1a shows the simulated electric field amplitude map of the SPP mode excited at normal incidence at 490 nm (E_y component) for a bare Ag grating in air with the following geometric parameters of the grating: period = 420 nm, duty ratio = 0.64, height = 20 nm. Fig. 1b shows a scanning electron micrograph of the experimental grating fabricated by LIL on a PET substrate. The simulated and experimental reflectance spectra for this grating are shown, along with the reflectance for a flat Ag electrode for comparison, in Fig. 1c. While the flat Ag electrode only exhibits absorption in the ultraviolet, the nanostructured grating electrode shows a clear reflectance dip at 490 nm due to the light coupling into the SPP mode, as shown in Fig. 1a. The good match in the position of the dip between measurement and simulation verifies that the SPP mode is excited on the grating surface as predicted. We note that the dip of the measured reflectance spectrum is shallower than that predicted (see Fig. 1c). We attribute this to the light scattering by the surface and line edge roughness of the fabricated grating, also seen in the micrograph of Fig. 1b, that somewhat diminish the quality and photonic properties of the structure. As we will discuss below, this is also manifested in a measured EQE enhancement that is smaller than predicted theoretically.

3.2. Simulated optical properties of complete device stack

Simulations confirm that the SPP mode of the bare Ag grating shifts to longer wavelengths when a higher index material (namely the active layer of the device in this study) is deposited onto the grating. This results in a SPP mode that is predominantly confined within the active layer (Fig. 2a) and is centered at 875 nm

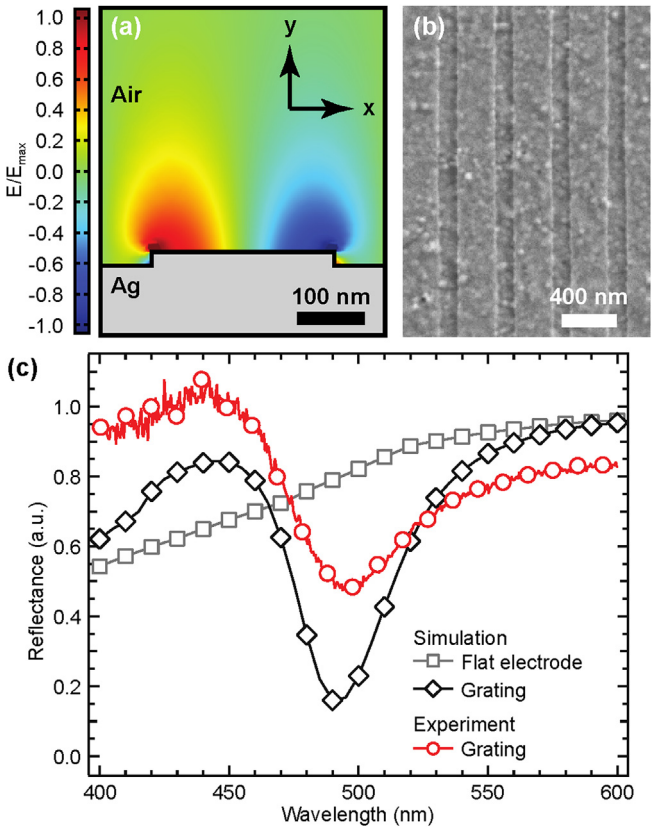

Fig. 1. (a) Normalized electric field (E_y) amplitude map for normal incidence excitation of the SPP mode at 490 nm of a bare Ag grating in air. (b) Scanning electron micrograph of the experimental Ag grating fabricated on a PET substrate. (c) Simulated and experimental reflectance spectra for the bare Ag grating in air, with the reflectance of a flat Ag electrode for comparison.

(Fig. 2b). The mode profile that stretches out into the active layer is a characteristic feature of a SPP mode. In contrast, LSPR modes tend to exhibit much smaller mode volume with only small spatial overlap with the active layer [27]. Fig. 2b shows the simulated absorption by the P3HT:PCBM active layer in devices containing either a flat Ag electrode or the nanostructured Ag grating electrode. For the device with the nanostructured Ag grating electrode, simulated spectra are shown for transverse magnetic (TM) and transverse electric (TE) polarization of the incident light (i.e., parallel to and perpendicular to the grating period, respectively). Fig. 2b highlights that the SPP mode results in significant enhancement of the subgap absorption (Fig. 2c). The dispersion curves calculated by the finite-difference time-domain method for TM polarization further confirmed that the plasmon mode in our device is the SPP mode propagating along the surface (Fig. S2; Supporting Information). Fig. 2b also shows two waveguide modes, which are excited depending on the orientation of the incident light polarization relative to the period of the grating, that also result in a slight enhancement of the predicted absorption. The position of the modes in the NIR is outside the normal absorption of P3HT and PCBM (although the blend exhibits an absorption due to the charge-transfer state formed at the donor-acceptor interface [9]) and is therefore a suitable choice for exploring enhancement of the EQE in the subgap spectral region. Fig. 2c shows the predicted absorption enhancement for the active layer with the nanostructured grating relative to the equivalent device with a standard flat electrode, suggesting that the absorption could be enhanced by up to a factor of ca. 8 due to the coupled SPP mode.

3.3. Fabrication and performance of grating-enhanced OPV device

Following the theoretical design and fabrication of the Ag grating, a method is needed to integrate the grating as an electrode (with additional photonic properties) into an OPV device. We have previously demonstrated air-processed organic photodiodes fabricated with a hot press lamination process with performance matching or slightly exceeding that of devices with thermally evaporated (flat) Ag electrodes [23]. That study was motivated by the need to integrate pre-fabricated top electrodes onto OPV devices, and showed that a conducting adhesive interlayer is necessary to create a mechanically and electrically robust contact between Ag and the P3HT:PCBM layer [23]. We have previously used PEDOT:PSS with a small amount (10% by liquid weight) of d-sorbitol, which acts as a “conducting glue” [24], when spin-coated onto a Ag film on PET [23].

Here we use the same lamination technique to integrate Ag gratings and flat Ag controls onto OPV devices, albeit with a significant modification compared to previous work. Our simulations indicated that the mismatch in the refractive index between the PEDOT:PSS and the P3HT:PCBM layers [16,28,29] would result in optical losses owing to undesirable light confinement in the PEDOT:PSS layer. The simulated resonance SPP mode shown in Fig. 2, which assumes direct contact of the Ag grating and the active layer, will essentially collapse into the PEDOT:PSS layer if such a low index layer is added between the grating and the active layer. In order to circumvent this situation and allow the optical field to extend through the thickness of the active layer as shown in Fig. 2a, the refractive indices of the adhesive layer and the active layer need to be matched. We found here that a thin layer of P3HT, mixed with d-sorbitol to improve adhesion, worked as an index-matched adhesive interlayer. In this work, our best devices were optically optimal at an expense of a sub-optimal electrical performance (J_{sc}: 7.1 mA/cm^2, V_{oc}: 450 mV, *FF*: 44%, *PCE*: 1.4%). The lower performance compared to optimized P3HT:PCBM-based devices with a PEDOT:PSS/Ag top contact is attributed to the reduced electrical conductivity in P3HT that increases series resistance losses, in addition to energy mismatch between the work function of Ag and the HOMO level of P3HT as compared to the conducting polymer PEDOT:PSS treated with d-sorbitol [30]. However, the P3HT-based interlayer allows us to demonstrate how a nanostructured-Ag electrode can effectively be incorporated into an optoelectronic device using a simple methodology.

We measured the external quantum efficiency (EQE) of our devices with flat and nanostructured-Ag electrodes in the 300 nm–1000 nm range (Fig. 3a). Both devices were fabricated side-by-side with the same lamination procedure described above. While the devices show similar performance between 300 and 600 nm (there may be a small decrease in the EQE, which could be due to small differences in the active layer thickness), of importance to our present study is the optical response of devices in the NIR region. We observe a distinct peak in the EQE at ca. 840 nm and a shoulder at 780 nm from the device with nanograting Ag electrode while they are not present in the control device with a flat Ag electrode. In Fig. 3b we show the EQE enhancement factor, defined as the ratio between the EQE of the device with the Ag nanograting electrode and that of a device with a flat Ag control, in this spectral range.

To verify that the observed EQE enhancement originates from SPP excitation in the grating, we measured EQE spectra with linearly polarized light. When the polarization is parallel to the period of the grating (i.e., TM; perpendicular to the grating lines), excitation of SPP modes is expected and indeed we observe the maximum EQE enhancement as shown in Fig. 3b (right panel). In the case when the light is polarized perpendicular to the period of

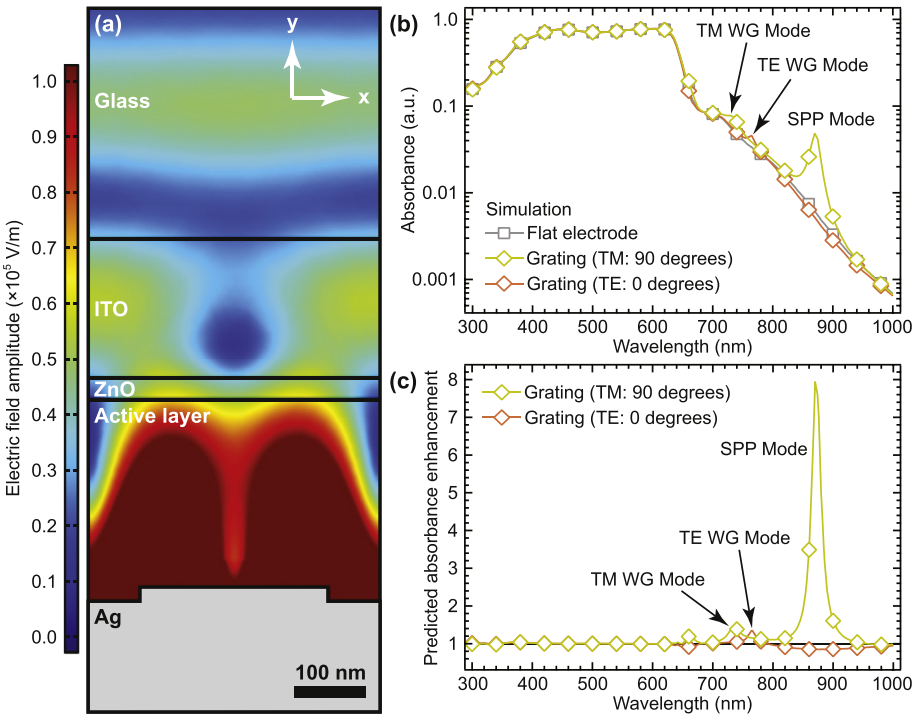

Fig. 2. (a) Electric field amplitude map for normal incidence excitation of the SPP mode at 875 nm. (b) Simulated absorbance spectra as a function of the incident light polarization relative to the grating period, for the active layer in a complete device stack incorporating the same Ag grating, with the corresponding absorbance for a device with a flat Ag electrode for comparison. (c) The predicted polarization-dependent absorbance enhancement as a result of incorporating the nanostructured Ag grating electrode.

the grating (i.e., TE; parallel to the grating lines) the SPP modes should not be excited, but measurable EQE enhancement is still observed. In fact, when the light is polarized at 45° to the period of the grating, the EQE enhancement shown in Fig. 3b (center) is comparable to the case when the light should be most strongly coupled to the SPP mode. Although, the TE waveguide mode contributes a small amount of absorption enhancement for non-optimal incident light polarization, we attribute these observations to imperfections in the grating and to the fact that light is not perfectly polarized along the plane shown. The imperfection of the fabricated grating, evident in the SEM image of Fig. 1b, is also responsible for the reduced magnitude of the measured enhancement of the EQE with respect to the calculated enhancements of the order of 50 [16]. Improving both the quality of the starting Ag film and the quality of the resulting Ag nanograting should result in higher enhancement. Nevertheless, the observed factor of ca. 5 enhancement of the EQE clearly demonstrates that nanostructured metal gratings can be used as "photonic electrodes" that can enhance targeted optical modes in the device.

The calculated SPP mode at 875 nm, shown in Fig. 2, matches well with the measured EQE enhancement factor peaking at 830 nm. Since the theoretical and experimental resonance peak position in the reflectance spectrum of the bare grating in Fig. 1c were in excellent agreement, we argue that the discrepancy between the simulated and measured peak positions in the full device is due to uncertainty in the optical parameters for the dielectric stacks. For example, only a five percent decrease in the refractive index of the P3HT:PCBM layer will blue-shift the SPP resonance more than 30 nm. Such an error in the assumed refractive index is readily explained from the uncertainty in the measurement of the layer thicknesses in the reference samples. In addition, the geometric imperfections of the Ag grating can also affect the position of the SPP mode in the presence of a higher refractive index medium.

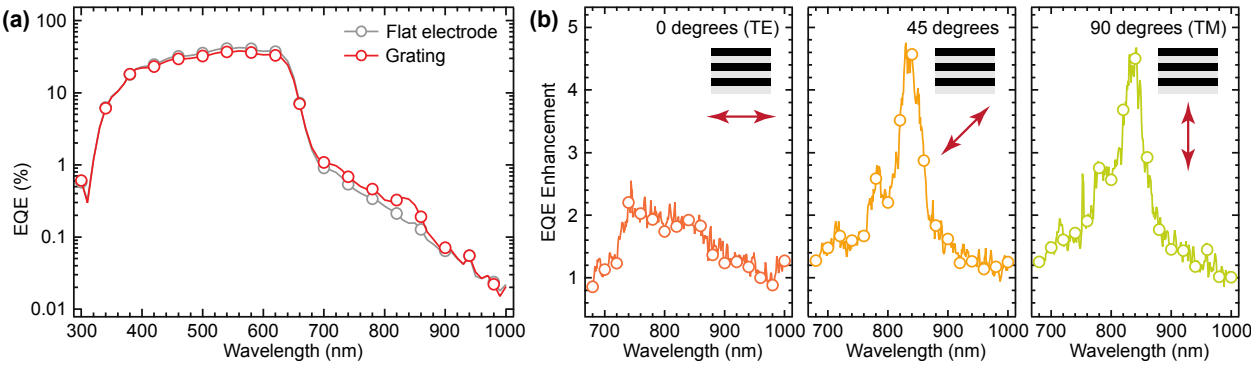

Fig. 3. (a) Experimentally measured EQE for the device containing the nanograting Ag electrode and a reference device containing a flat Ag electrode and (b) device EQE enhancement factor (see text for definition) for normal incidence with polarization parallel (TE; left) and perpendicular to the period of the grating (TM; right).

4. Conclusions

Our results demonstrate a proof-of-concept in which we were able to enhance the photoresponse of a single junction OPV device in the NIR region where the active layer materials do not normally absorb light. We do this without the development of new red-absorbing materials or the fabrication of multi-junction structures. Our modular lamination approach allows the individual processing of the device components that are subsequently brought together. As such, organic semiconducting materials do not have to be subjected to harsh processing environments required for creating nanostructures on their surface in order to accomplish photonic enhancement in the device. Additionally, the lamination process provides a means by which the active components of the device stack are encapsulated, limiting access of the ambient environment that might result in device degradation and loss of performance. We show good agreement between the spectral position of the measured EQE enhancement and the predicted SPP mode in the optical absorption spectrum of the device stack. This result confirms that the nanostructured-Ag electrode enhances light trapping in the active layer and thus effectively increases the optical field intensity at specific resonance wavelengths. We show that CT states excited by the trapped NIR modes create free charges that can now be harvested and contribute to the enhanced EQE when the nanograting electrode is used.

We note that our proof-of-concept device uses a simple grating with a single period along one dimension of its surface. While this still allows much flexibility in tuning excitation of modes within a desired spectral range [16], one can envision coupling our lamination-based strategy with elaborate two-period or semi-periodic metal nanostructures to excite multiple modes or even achieve broadband enhancement of the photoresponse of thin film photovoltaic devices [21].

Acknowledgments

We would like to thank Dr. Paul Ndione for his help with variable-angle spectroscopic ellipsometry measurements of the optical properties. AMN and SA have contributed equally to this work. This work was supported by the U.S. Department of Energy (DOE) under Contract No. DE-AC36-08GO28308 with the National Renewable Energy Laboratory. Funding provided by DOE's Advanced Research Projects Agency – Energy (ARPA-E) under Grant Number DE-AR0000289. The U.S. Government retains and the publisher, by accepting the article for publication, acknowledges that the U.S. Government retains a nonexclusive, paid-up, irrevocable, worldwide license to publish or reproduce the published form of this work, or allow others to do so, for U.S. Government purposes.

Appendix A. Supplementary data

Supplementary data related to this article can be found at http://dx.doi.org/10.1016/j.orgel.2016.09.011.

References

[1] J.W. Jung, J.W. Jo, E.H. Jung, W.H. Jo, Org. Electron. 31 (2016) 149.
[2] S. Zhang, L. Ye, J. Hou, Adv. Energy Mater. 6 (2016), http://dx.doi.org/10.1002/aenm.201502529.
[3] Q. Gan, F.J. Bartoli, Z.H. Kafafi, Adv. Mater. 25 (2013) 2385.
[4] C.-H. Chou, F.-C. Chen, Nanoscale 6 (2014) 8444.
[5] S. Ahn, D. Rourke, W. Park, J. Opt. 18 (2016) 033001.
[6] C.-M. Yang, P.-Y. Tsai, S.-F. Horng, K.-C. Lee, S.-R. Tzeng, H.-F. Meng, J.-T. Shy, C.-F. Shu, Appl. Phys. Lett. 92 (2008) 083504.
[7] K. Vandewal, A. Gadisa, W.D. Oosterbaan, S. Bertho, F. Banishoeib, I. Van Severen, L. Lutsen, T.J. Cleij, D. Vanderzande, J.V. Manca, Adv. Funct. Mater. 18 (2008) 2064.
[8] T. Drori, C.X. Sheng, A. Ndobe, S. Singh, J. Holt, Z.V. Vardeny, Phys. Rev. Lett. 101 (2008) 037401.
[9] K. Vandewal, K. Tvingstedt, A. Gadisa, O. Inganas, J.V. Manca, Nat. Mater. 8 (2009) 904.
[10] J.-L. Wu, F.-C. Chen, M.-K. Chuang, K.-S. Tan, Energy Environ. Sci. 4 (2011) 3374.
[11] K. Vandewal, S. Albrecht, E.T. Hoke, K.R. Graham, J. Widmer, J.D. Douglas, M. Schubert, W.R. Mateker, J.T. Bloking, G.F. Burkhard, A. Sellinger, J.M.J. Frechet, A. Amassian, M.K. Riede, M.D. McGehee, D. Neher, A. Salleo, Nat. Mater. 13 (2014) 63.
[12] L.J.A. Koster, S.E. Shaheen, J.C. Hummelen, Adv. Energy Mater. 2 (2012) 1246.
[13] J.K. Mapel, M. Singh, M.A. Baldo, K. Celebi, Appl. Phys. Lett. 90 (2007) 121102.
[14] M.E. Sykes, A. Barito, J.A. Amonoo, P.F. Green, M. Shtein, Adv. Energy Mater. 4 (2014) 1301937.
[15] M.A. Sefunc, A.K. Okyay, H.V. Demir, Opt. Express 19 (2011) 14200.
[16] D. Rourke, S. Ahn, A.M. Nardes, J. van de Lagemaat, N. Kopidakis, W. Park, J. Appl. Phys. 116 (2014) 114510.
[17] K. Tvingstedt, N.-K. Persson, O. Inganas, A. Rahachou, I.V. Zozoulenko, Appl. Phys. Lett. 91 (2007) 113514.
[18] X.H. Li, W.E.I. Sha, W.C.H. Choy, D.D.S. Fung, F.X. Xie, J. Phys. Chem. C 116 (2012) 7200.
[19] J.B. Kim, P. Kim, N.C. Pégard, S.J. Oh, C.R. Kagan, J.W. Fleischer, H.A. Stone, Y.-L. Loo, Nat. Photonics 6 (2012) 327.
[20] J. You, X. Li, F.-X. Xie, W.E.I. Sha, J.H.W. Kwong, G. Li, W.C.H. Choy, Y. Yang, Adv. Energy Mater. 2 (2012) 1203.
[21] X. Li, W.C.H. Choy, X. Ren, J. Xin, P. Lin, D.C.W. Leung, Appl. Phys. Lett. 102 (2013) 153304.
[22] J. van de Groep, D. Gupta, M.A. Verschuuren, M.M. Wienk, R.A.J. Janssen, A. Polman, Sci. Rep. 5 (2015) 11414.
[23] B.A. Bailey, M.O. Reese, D.C. Olson, S.E. Shaheen, N. Kopidakis, Org. Electron. 12 (2011) 108.
[24] J. Huang, G. Li, Y. Yang, Adv. Mater. 20 (2008) 415.
[25] M. Campbell, D.N. Sharp, M.T. Harrison, R.G. Denning, A.J. Turberfield, Nature 404 (2000) 53.
[26] S. Ahn, S. Kim, H. Jeon, Appl. Phys. Lett. 96 (2010) 131101.
[27] D. Lu, E. Rengnath, Y. Cui, Z. Wang, Y. Ding, W. Park, Appl. Phys. Lett. 102 (2013) 241114.
[28] H. Hoppe, N. Arnold, D. Meissner, N.S. Sariciftci, Thin Solid Films 451-452 (2004) 589.
[29] A.J. Moule, J.B. Bonekamp, K. Meerholz, J. Appl. Phys. 100 (2006) 094503.
[30] A.M. Nardes, M. Kemerink, M.M. de Kok, E. Vinken, K. Maturova, R.A.J. Janssen, Org. Electron. 9 (2008) 727.